Author version: Paleoceanography, vol.25; 11 pp, doi:10.1029/2008PA001687

Evaporation-Precipitation Changes in the Eastern Arabian Sea for the last 68 ka: Implications on Monsoon Variability

Pawan Govil[1,2], Pothuri Divakar Naidu[1]

1. National Institute of Oceanography (CSIR), Dona Paula, 403 004, Goa, India.
2. National Centre for Antarctic and Ocean Research, Headland Sada, Vasco-da-Gama, 403 804, Goa, India.

Abstract

Variations in sea surface temperature (SST), $\delta^{18}O$ of sea water ($\delta^{18}Ow$) and salinity were reconstructed for the past 68 ka using a sediment core (AAS9/21) from the Eastern Arabian Sea (EAS) in order to understand the changes in evaporation and precipitation associated with the monsoon system. The Mg/Ca derived SST record varies by ~4^0C; it shows that marine isotope stage (MIS) 4 was warmer than MIS3, that the last glacial maximum (LGM) was 4^0C cooler than the present, and there was a 2^0C increase within the Holocene. MIS4 records higher $\delta^{18}Ow$ and salinity values than MIS2, suggesting variable flow of low salinity Bay of Bengal flow into the EAS during glacial periods. The transition from MIS4 to MIS3 was marked with a conspicuous shift from higher to lower $\delta^{18}O_W$ values, which reflects a decrease in the evaporation-precipitation budget in the EAS, perhaps due to the strengthening of southwest (SW) monsoon. Monsoon reconstructions based on $\delta^{18}Ow$ reveal that monsoon driven precipitation was higher during MIS3 and MIS1, and lower during MIS2 and MIS4. This is consistent with earlier monsoon reconstructions based on upwelling indices from the western Arabian Sea. However, the amplitude of monsoon fluctuations derived through upwelling indices and $\delta^{18}O_W$ varies significantly, which may indicate spatial variability of monsoon rainfall.

1. Introduction

The southwest (SW) monsoon emanate from the temperature and pressure gradients that occur between the Indian Ocean and Tibet Plateau during the summer. The upper ocean heat supplies the necessary evaporation and atmospheric moisture transport during this phenomenon. Consequently, a strong link exists between ocean dynamics and the atmospheric heat and moisture transfer behind the monsoon [*Shukla and Mooley*, 1987; *Rao and Goswami*, 1988; *Webster et al.,* 1998]. Indeed, there is a strong coupling between the water (evaporation-precipitation) and heat budgets of the Arabian Sea and the intensity of the SW monsoon. The socio-economic and agriculture development of southeast Asia depend on the monsoon precipitation from June through September, which contributes about 70 to 90% of the annual precipitation in the region. Therefore, an understanding of the monsoon system beyond historical records is desired.

For the last two decades, reconstructions of monsoon variability on glacial, interglacial and millennial time scales have been carried out using sediment cores from the western Arabian Sea (WAS). Most of these are based on indices for upwelling [*Prell,* 1984; *Anderson and Prell,* 1993; *Sirocko et al.*, 1993; *Naidu and Malmgren,* 1995; 1996; *Overpeck et al.*, 1996; *Altabet et al.*, 2002; *Gupta et al.*, 2003; *Naidu,* 2004]. However, such monsoon reconstructions effectively represent the SW monsoon wind strength rather than precipitation [*Sarkar et al*., 2000]. Rather, precipitation depends on the moisture transport from the southern Indian Ocean [*Webster et al*., 1998; *Ramesh kumar and Schlussel*, 1998].

Although the eastern Arabian Sea (EAS) receives more precipitation than the WAS during the SW monsoon [*Ramesh Kumar and Prasad*, 1977], only limited studies have assessed monsoon variability in the EAS [*Sarkar et al.*, 1989; *Reichart et al*., 1998, *Schulz et al*., 1998, *Sarkar et al.*, 2000; *Chodankar et al.*, 2005; *Tiwari et al.*, 2005a]. A few researchers have used organic carbon in sediment as a proxy for past monsoon strength and associated oxygen minimum zone variability [*Reichart et al*., 1998, *Schulz et al*., 1998]. Others have used the oxygen isotope ratios of planktic foraminifera tests [*Sarkar et al.*, 2000; *Thamban et al*., 2001; *Chodankar et al*., 2005; *Tiwari et al.*, 2005a]. However, the oxygen isotope ratios of planktic foraminifera are controlled by several factors including global variation of δ^{18}Ow due to growth and decay of continental ice sheets and by local sea surface temperature (SST) and sea surface salinity, the latter linked to the local evaporation-precipitation balance. Hence, without accounting contributions of continental ice volume, local SST and sea surface salinity, the δ^{18}O values of planktic foraminifer tests in terms of precipitation variability remain uncertain. Attempts have been made to extract the SST component of planktic foraminifer δ^{18}O from cores in the EAS using alkenone unsaturation ratios [*Rostek et al*., 1993, 1997]. However, seasonal abundances of planktic foraminifera and alkenone producing coccoliths may differ, such that SST and δ^{18}Ow reconstructions need to be confirmed by other methods.

Paired measurements of Mg/Ca and δ^{18}O in selected planktic foraminifera species can be used to reconstruct SST and δ^{18}Ow in the Arabian Sea [*Dahl and Oppo*, 2006; *Saher et al*., 2007; *Anand et al*., 2008]. The

$\delta^{18}O_W$ values, after correction for continental ice volume, may then be a reliable proxy for monsoon variations because $\delta^{18}O_W$ is influenced by evaporation and precipitation in this region [*Sarkar et al*., 2000]. Here, we use this approach to address the evaporation-precipitation budget and monsoon variability from a sediment core from the EAS (Figure 1) covering a time span of last 68 ka.

2. Regional Oceanography

Seasonal reversals of SW and NE monsoon winds over the Arabian Sea affect surface circulation, productivity, biogenic and lithogenic fluxes, CO_2 uptake and the heat budget in the region. In response to strong SW monsoon winds during June through September, intense upwelling occurs off the coasts of Somali and Oman due to wind-induced offshore Ekman transport [*Wyrtki*, 1973]. During this season, upwelling of cool waters leads to enhanced heat loss in the WAS, which is characterized by a ~4°C SST gradient from the west to the east [*Levitus and Boyer, 1994]* (Figure 2a).

Most of the SW monsoon precipitation on the Western Ghats drains into the Arabian Sea through numerous rivers and streams contributing to the local formation of low salinity waters with a gradient from near shore to offshore (Figure 2b). As a consequence of SW monsoon precipitation and associated river run low δ^{18}Ow values near to the shore and higher δ^{18}Ow values in the offshore were noticed in the EAS (Figure 2c) [Joint Global Ocean Flux Study data set in *Dahl and Oppo*, 2006]. In contrast, during NE monsoon about 6 Sv of low saline waters of Bay of Bengal flows into the EAS [*Shankar et al*., 2002], which decreases salinity in the EAS [*Wyrtki*, 1973: *Levitus and Boyer*, 1994]. Both box model and numerical circulations models demonstrate that low δ^{18}O–salinity slope (0.26) in the Arabian Sea is due to evaporation-minus-precipitation balance [*Delaygue et al*., 2001]. Therefore, the general pattern of evaporation and precipitation in the EAS is influenced by heavy precipitation during SW monsoon and cooling during NE monsoon [*Hasternath and Lamb*, 1979].

3. Material and Methods

3.1 Core and chronology

Sediment core AAS9/21 was collected at 1807m water depth in the EAS (14° 30.539' N, 72° 39.118'E) (Figure 1) during *A. A. Sidorenko* cruise 9. Core AAS9/21 was 4.2 m long and consists of a mixture of terrigeneous and biogenous material. The terrigeneous material comprises clay and silt, whereas the biogenous material consist of planktic and bethic foraminifera and traces of pteropods and diatoms. The chronology of this core to 310 cm depth was established based on six AMS ^{14}C dates. Below, the chronology was established by correlating our δ^{18}O of *Globigerinoides ruber* record with the low latitude global isostack curve of *Martinson et al.* [1987].

AMS ^{14}C dating was performed on monospecific samples of the planktic foraminifera *G. ruber* using the Tandem Accelerator at Leibniz Labor fur Altersbestimmung und Isotopenforschung, Christian-Alberchts-Universitat, Kiel, Germany. Measured ^{14}C ages were converted to sediment ages using the online CalPal version quickcal 2005 ver1.4 [*Weninger et al.*, 2006]. Before calibration, radiocarbon dates were corrected for a reservoir effect (400 years) based on observations for the Indian Ocean [*Southon et al.,* 2002]. Sedimentation rate varies from 4.6 to 13.6 cm/kyr at this core location (Figure 3).

3.2 Mg/Ca analyses and estimation of temperature

For determination of Mg/Ca, 30 to 40 individuals of planktic foraminiferal species *G. ruber* (white variety) with a size range of 250 to 350µm were picked and gently crushed while viewed with a binocular microscope. Care was taken not to pulverize broken shell fragments. Clay lumps and shell fragments containing clays were removed manually. Crushed samples were cleaned following the protocol described in *Barker et al*. [2003]. 500 µl of 0.075M HNO_3 was added to cleaned samples and left overnight to dissolve foraminiferal shell fragments completely. Solutions were transferred into clean vials and diluted with 0.001M HNO_3 to make a ~1 ml solution for analyses. Mg and Ca analyses were carried out on a Thermo Finnigan Element2 sector field inductively coupled plasma mass spectrometer. Elemental concentrations were derived from the isotopes ^{25}Mg and ^{43}Ca; ^{89}Y served as internal standard. ^{27}Al, and ^{55}Mn were also routinely measured simultaneously to monitor the effectiveness of the cleaning protocol. The analytical error for Mg/Ca was better than 0.7%. 40 sample solutions were measured in replicate on different days and found that repeatability for Mg/Ca was $\pm$0.1mmol/mol (1σ).

SST was estimated using a relationship obtained from core-tops from the North Atlantic [*Dekens et al.,* 2002]: Mg/Ca = 0.38exp(0.09 (SST)), where Mg/Ca is in mmol/mol and SST is in °C. This calibration equation was selected because derived temperatures of the core tops were close to modern values at the core location, which is within error estimate of $\pm$0.3°C.

3.3 Oxygen isotope analyses

For the $\delta^{18}O$ analyses, new splits of cleaned *G. ruber* specimens (250 to 350µm size range) were analysed using a Finnigan MAT 252 mass spectrometer equipped with an automatic carbonate preparation device at the Universität Bremen, Germany. The mean external error and reproducibility (1σ) of carbonate standard is better than $\pm$0.07‰ and $\pm$0.05‰ for $\delta^{18}O$ and $\delta^{13}C$, respectively. Oxygen and carbon isotopic values are expressed as per mil (‰) deviation Vienna Pee Dee belemnite (VPDB) standard, calibrated by NBS 18, 19 and 20 standards.

3.4 Estimation of $\delta^{18}Ow$ from Mg/Ca and $\delta^{18}Oc$

Measured foraminiferal values ($\delta^{18}Oc$) were corrected for continental ice volume using an established data set [*Shackleton,* 2000]. A spline interpolation was made from our $\delta^{18}O$ data at 1 ka intervals. The "ice volume" values were then subtracted to obtain a residual $\delta^{18}O$. The independent time control and time resolution of the two data sets appear sufficient for this procedure. Residual $\delta^{18}O$ values were then used to compute a local $\delta^{18}O_W$ using the Mg/Ca derived SST by applying the following equation of *Bemis et al.* [1998]: $\delta^{18}O_W$ =0.27+((T-16.5+4.8*δ^{18}C)/4.8). Based on the error estimates of Mg/Ca analyses and $\delta^{18}Oc$, an overall error estimate (1σ) for reconstructed $\delta^{18}Ow$ is $\pm$0.1‰. $\delta^{18}O_W$ values were converted into salinity by using an equation given by *Dahl and Oppo* [2006]: S = ($\delta^{18}Ow$ + 20)/ 0.57. The relationship between $\delta^{18}Ow$-salinity depends on mixing of oceanic and fresh water end members. The fresh water component consists of a balance between evaporation, precipitation and continental run off. It is expected that, in the Arabian Sea, the fresh water component is tightly coupled with monsoon variability.

4. Results

4.1. *Oxygen isotopes*

The $\delta^{18}Oc$ values range from -2.3 to 0.2‰ over last 68 ka at the study site (Figure 4a). During MIS4, $\delta^{18}Oc$ values vary from -0.92 to -0.55‰ with an average value of 0.76‰. These are from -1.40 to -0.37‰ with an average value of -1.11‰ during MIS3. The $\delta^{18}Oc$ values do not show any major shifts (>1‰) within MIS3 and MIS4, whereas during MIS2 there is an abrupt $\delta^{18}Oc$ shift of 1‰ around 20 ka. From 19 to 7.5 ka, $\delta^{18}Oc$ decreases by 2.2‰ (Figure 4a). Despite considerable differences in time resolution, the $\delta^{18}Oc$ record of AAS9/21 compares fairly well with that at MD900963 [*Rostek et al.*, 1993].

4.2. Sea surface temperature

SST, based on Mg/Ca, decreased gradually from MIS4 to MIS2 (Figure 5a). During MIS4, SST ranges from 26.6 to 28.1^{0}C, reflecting a variation of 1.5^{0}C. SST varied from 25.2 to 27.1^{0}C during MIS 3, revealing that MIS4 was warmer than MIS3. During MIS2, SST varied from 27.3 to 24.5^{0}C with two brief warmings at ~20 and ~17 ka. SST varied from 27 to 29^{0}C at this core location during MIS1.

SST variations of AAS9/21 can be compared with other published SST records at ODP Site 723 and Core NIOP929 from the WAS, and Core SK17 from the EAS (Figure 5). Two brief warm excursions (ASW1 and ASW2) have been documented during MIS2 in these other records, indicating that these were regional features in the Arabian Sea. ODP Site 723, NIOP 929 and SK17 are located below regions of upwelling, so they generally record lower SST than AAS9/21 for the last 20 ka.

4.3. Oxygen isotope ratios of surface waters ($\delta^{18}Ow$)

During MIS4, δ^{18}Ow values range from 0.9 to 1.4‰, whereas during MIS3 they vary from 0.3 to 1.0‰. Strikingly, the δ^{18}Ow values are higher during MIS4 as compared to MIS2 (Figure 6a). Within MIS 2, the δ^{18}Ow record shows significant fluctuations of about 1‰ around 20 ka and 17 ka, which coincides with the timing of the warm events reported for the WAS [S*aher et al.*, 2007]. Between 20 and 17 ka, the highest δ^{18}Ow values were documented, and these are as high as modern values. During MIS 1, δ^{18}Ow varies from 1.08‰ to 0.2‰ (Figure 6a). Similarly, another core, SK17 from the EAS, also shows significant δ^{18}Ow fluctuations during MIS 2 (Figure 6b), which may coincide with ASW1 and ASW2. Although there are considerable differences in the sample resolution between AAS19/21 and SK17, the trends and fluctuations of δ^{18}Ow are comparable in these two cores over the last 30 ka.

4.4. Sea surface salinity

Sea surface salinity at the core location is varied by 2.1 psu over the last 68 ka (Figure 6a). Highest salinity (>36.8 psu) occurred during MIS4 and lowest salinity (<37 psu) occurred during MIS3 and MIS1. Minimum and maximum fluctuations of salinity were noticed during MIS3 and MIS4, respectively (Figure 6a). During MIS1, salinity values decreased from 10 to 3 ka, and increased from 3 ka onwards.

5. Discussion

5.1. Salinity Contrast Between Marine Isotope Stages 4 and 2

Our records from Core AAS9/21 indicate higher SSTs, enriched δ^{18}Ow and greater salinity during MIS4 (59-67 ka) compared to during MIS2 (Figures 4-6). Variations in δ^{18}Ow and salinity in this region are strongly coupled to one another, to the balance of evaporation and precipitation (E-P) [*Cadet and Reverdin,* 1981], and to the flow of Bay of Bengal water [*Levitus and Boyer*, 1994]. The observed contrast between the δ^{18}Ow of MIS4 and of MIS2, therefore, might be caused due to increased evaporation and/or decreased precipitation during MIS4 relative to MIS2, and/or greater flow of low salinity Bay of Bengal water during MIS2.

The strength of the SW monsoon appears to have been weaker during MIS2 than during MIS4 [*Anderson and Prell*, 1993], Consequently, evaporation was probably higher during MIS2 [*Rostek et al.,* 1993], such that a reduced E-P budget during MIS4 compared to MIS2 seems unlikely. In view of this, we favor a change in the flow of Bay of Bengal water to explain the salinity contrast. During the NE monsoon, about 6 Sv of Bay of Bengal water enter the EAS [*Shankar et al*., 2002], with much of this flow confined to the western continental margin of India where the core is located. Strong NE monsoon winds during MIS2 [*Duplessy et al*., 1982; *Sarkar et al*., 1989] would have increased the flow of less saline Bay of Bengal water into the EAS whereas relatively weak NE monsoon winds during MIS4 would result in the opposite. By contrast, records from Core MD900963 suggest higher sea surface salinity during MIS2 than during MIS4 [*Rostek et al.*, 1993]. This difference may reflect the proximity of core locations to the low salinity water mass of the Bay of Bengal. Specifically, Core MD900963 is located further south from the path of low saline water.

5.2. Marine Isotope Stage 3

The transition from MIS4 to MIS3 shows a clear shift from high to low $\delta^{18}O_w$ values (Figure 6). We take this as representing a reduced E-P budget in the EAS, which may be due to a stronger SW monsoon during MIS3. Monsoon variability records, based on upwelling indices from the WAS [*Anderson and Prell*, 1993] or on productivity records from the Pakistan Continental Margin [*Schulz et al.*, 1998], also support a more intense SW monsoon during MIS3 compared to MIS4. This would have led to more precipitation and less evaporation during MIS3. In fact, at times, $\delta^{18}O_w$ values during MIS3 are similar to modern values, which may indicate that SW monsoon precipitation during MIS3 was as strong as at present-day.

Strikingly, SST values were lower during MIS3 than during MIS4 (Fig. 5a). The same result was inferred from analyses of Core MD900963 [*Rostek et al.*, 1993], suggesting that a broad area of the EAS was cooler during MIS3 than during MIS4. However, the increase in $\delta^{18}O_w$ values between 32.5 to 24.5 ka (Figure 6a) could be due to less precipitation caused by a weak SW monsoon.

5.3. Marine Isotope Stage 2

A 3^0C SST variation occurred during MIS2 with a minimum value of 24.5^0C during the last glacial maximum (LGM) and a maximum value of 27.5^0C at the boundary between MIS2 and MIS1 (Figure 5). The EAS was therefore 4^0C cooler during the LGM than during most of the Holocene (Figure 5a). Such cooling during the LGM is much greater than that inferred previously from some SST records generated using foraminifera assemblages (1-2^0C) [*CLIMAP*, 1981; *Naidu and Malmgren*, 2005], or alkenones (2^0C) [*Rostek et al*., 1993; 1997; *Emeis et al*., 1995; *Banakar et al*., 2005]. It is argued here that the deviation reflects location, specifically that earlier records come from regions of upwelling, where variability during the SW monsoon impacts SST. For example, both Core SK17 and Core AAS9/21 are located in the EAS. However, Core SK17 is located below the modern upwelling cell produced during the SW monsoon, whereas Core AAS9/21 is located further offshore where upwelling does not occur during any season. Consequently, SSTs should increase more over last 30 ka in Core AAS9/21; that is, this core should provide a better regional SST shift between the LGM and the Holocene in the Arabian Sea. We also note that alkenone based SST records from the EAS [e.g., *Rostek et al.*, 1997; *Banakar et al*., 2005] underestimate the SST shift between the LGM and the Holocene due to the seasonality of alkenone-producing coccoliths, and the lateral transport of alkenone bearing fine-grained material from upwelling regions [*Saher et al*., 2009]. Importantly, the 4^0C difference between the LGM and present-day (Fig 4) does agree with results from some work in the EAS [*Dahl and Oppo*, 2006; *Anand et al*., 2008].

Various studies have demonstrated that the SW monsoon was weaker during the LGM than present-day [*Prell,* 1984; *Naidu and Malmgren*, 1995; *Overpeck et al.*, 1996; *Naidu*, 1998 and references therein]. On the other hand, the NE monsoon may have been stronger during the LGM [*Duplessy*, 1982]. The flow of low saline Bay of Bengal water into the Arabian Sea depends on the strength of winter circulation [*Shankar et al*., 2002]. It has been found that this flow was higher during the LGM [*Sarkar et al.*, 1989], and that the NE monsoon was strengthened during early deglaciation around 18 ka [*Tiwari et al.*, 2005b]. The low $\delta^{18}O_W$ and salinity values between 19 and 18 ka are consistent with these inferences.

Excepting a brief interval of low $\delta^{18}O_W$ and sea surface salinity between 19 and 18 ka, these values were overall higher during MIS2 compared to MIS3. This suggests that the EAS experienced greater evaporation and less precipitation during MIS2 than during MIS3. Furthermore, greater amplitude fluctuations of $\delta^{18}O_W$ during MIS2 reflects that the strength of cold and dry NE monsoon winds has varied significantly resulting more evaporation variability and/or more flow of less saline Bay of Bengal waters to the EAS.

Comparison of $\delta^{18}O_W$ values between LGM and today in a suite of sediment cores across the Arabian Sea reveals that the EAS experienced almost no change in $\delta^{18}O_W$ during LGM relative to today [*Dahl and Oppo*, 2006]. The $\delta^{18}O_W$ values of the LGM in the present studied core and in Core SK17 from the EAS [*Anand et al*., 2008] also do not show significant differences with those of core tops.

5.4. Abrupt warm events within MIS2

During MIS2, two excursions to warmer SSTs occurred around 20 ka and 17 ka (Figure 5a). Similar warmings were identified in Core NIOP929 from the WAS, although there is an apparent $\pm$0.5 ka time difference between the records. These were termed Arabian Sea Warm Event 2 (ASW2) at 19 ka and Arabian Sea Warm Event 1 (ASW1) at 17 ka [*Saher et al.*, 2007]. Warm events seemingly corresponding to ASW2 and ASW1 were also found in SST records from ODP Site 723 and Core SK17 (Figures 5 b, d), suggesting that these are changes in regional conditions.

Saher et al [2007] have proposed three alternative mechanisms to explain the warm events in the Arabian Sea: (1) a reduction in upwelling intensity; (2) strong influence of NE monsoon, and (3) an increase in the influx of warm water into the Arabian Sea. The third mechanism might result from a merging of the Northeast Madagaskar Current (NEMC) and the East African Coast Current (EACC) due to increased trade wind intensity. That these events occurred in both the WAS and EAS (present study), the latter where significant upwelling does not occur and the influence of NEMC and EACC is at minimum, may indicate a link to changes in the NE monsoon. The intensity of the NE monsoon during glacial periods exerts a larger influence on Arabian Sea SSTs than during interglacial periods [*Duplessy,* 1982; *Fontugne and Dupless,y* 1986; *Prell and Vancampo*, 1986]. Accordingly, variation in NE monsoon intensity during glacials would cause greater amplitude SST fluctuations as compared to present condition in both WAS and EAS. However, the effect of NE monsoon winds must be more intense in the EAS and Bay of Bengal as compared to WAS [*Montegut et al.*, 2007]. Therefore, high magnitude fluctuations of $\delta^{18}O_W$ at this core site strongly suggest that the intensity of the NE monsoon and associated flow of Bay of Bengal waters into the EAS have varied largely due to stronger monsoon winds during MIS2 [*Duplessy*, 1982, *Prell and Vancampo*, 1986; *Sarkar et al.*, 1989]. Thus, a reduction of cold NE monsoon winds would have caused the two warm events (ASW1 and ASW2) in the Arabian Sea.

5.5. Marine Isotope Stage 1

During MIS1, about 2^0C of SST variation is documented at the core location (Figure 5a) but there is no long term cooling during late Holocene. This contrasts somewhat with the 0.5^0C change SST estimates during MIS1 based on alkenones from the EAS [*Rostek et al.*, 1993], and a late Holocene cooling at ODP Site 723 [*Naidu and Malmgren*, 2005]. Assuming no major temperature changes during MIS1, δ^{18}Oc variations during MIS1 in the EAS have been interpreted as representing changes in the intensity of SW monsoon [*Sarkar et al*., 2000; *Thamban et al*., 2001; *Tiwari et al*., 2005a]. A 2°C change in SST accounts a 0.5‰ change in δ^{18}O, which is significant, hence observed SST variability challenges the assumption. The lack of cooling during the late Holocene, in the present core and in Core SK17 [*Anand et al*., 2008], may suggest that the late Holocene cooling trend is restricted to the WAS [*Naidu and Malmgren*, 2005]. It may reflect increased upwelling in the WAS during Late Holocene.

In the MIS1, from 10.5 to 3 ka is marked by gradual decreasing trend of $\delta^{18}O_W$ and salinity values, which represent the increasing strength of SW monsoon during this period. From ~3.5 ka onwards enriched $\delta^{18}O_W$ and high salinity values are noticed (Figure 6a), which suggests that descending phase of SW monsoon initiated around this time. This increase in salinity and $\delta^{18}O_W$ is attributable to the onset of weak phase of SW monsoon around 3.5 ka due to arid climatic conditions in the Indian subcontinent. SW monsoon variability derived by $\delta^{18}O_W$ changes in the present study from the EAS is in consistent with the SW monsoon variability derived from upwelling indices from the western Arabian Sea [*Overpeck et al.*, 1996; *Naidu and Malmgren,* 1996] and δ^{18}O records of speleotherms from Oman [*Neff et al*., 2001] and δ^{18}Ow reconstructions from the Andaman Sea [*Rashid et al*., 2007] during the Holocene. However, the magnitude of fluctuations among these proxies such as upwelling indices, δ^{18}O of speleotherms and $\delta^{18}O_W$ differ significantly is attributable to spatial pattern of monsoon rainfall variability in the monsoon influenced regions.

6. Conclusions

We have reconstructed the SST and δ^{18}Ow from the EAS for the last 68 ka in order to understand evaporation and precipitation changes associated with SW and NE monsoons. Changes of δ^{18}Ow values reveal that more precipitation and less evaporation occurred during MIS1 and MIS3 due to strong SW monsoon, whereas more evaporation occurred during MIS2 and MIS4, probably because of stronger cold and dry NE winds blowing from the continent to the Arabian Sea. Furthermore, higher δ^{18}Ow values were noticed in MIS4 than in MIS2, suggesting greater inflow of Bay of Bengal water to the EAS during MIS2 compared to MIS4. The transition from MIS4 to MIS3 was marked with a conspicuous δ^{18}Ow shift, suggesting a shift from greater evaporation to greater precipitation in the EAS due to intensified SW monsoon rainfall.

The EAS was 4^0C cooler during LGM as compared to modern Holocene. The location of the core is not affected by upwelling and winter mixing. This may provide evidence for a regional SST shift between the LGM and the Holocene in the Arabian Sea. In this case, the earlier estimates for the change [e.g., CLIMAP, 1981] are too low. We note, though, that the SST of the EAS varied by 1 to 2^0C during glacials and interglacials.

Overall, the general trend of monsoon variability reconstructed based on the δ^{18}Ow values from the present study is in agreement with the monsoon reconstructions based on the upwelling indices from the western Arabian Sea, however the amplitude changes of monsoon variability based on upwelling indices and δ^{18}Ow vary strikingly in the early Holocene period could be due to spatial variability of rainfall in the region.

Acknowledgements

We thank Dr. Gerald Dickens, Editor for his thoughtful comments which significantly improved the readability and three anonymous reviewers for their constructive criticism, which ameliorated interpretation of the data presented in this paper. Part of this work was carried out during the tenure of DAAD fellowship to Dr. P. Govil at the University of Bremen, Germany. Dr. Stefan Mulitza has hosted Dr. P. Govil visit at the University of Bremen and Dr. Henning Kuhnert has provided analytical help in the laboratory. This work is supported by Ministry of Earth Sciences, New Delhi and ISRO-GBP program. This is National Institute of Oceanography Contribution…..

References

Altabet, M. A., M. J. Higginson, and D. W. Murray (2002), The effect of millennial-scale changes in Arabian Sea denitrification on atmospheric CO_2, *Nature*, *415,* 159–162.

Anand, P., D. Kroon, A. D.Singh, R. S. Ganeshram, G. Ganssen, and H. Elderfield (2008), Coupled sea surface temperature-seawater δ^{18}O reconstructions in the Arabian Sea at the millennial scale for the last 35 ka, *Paleoceanography*, *23*, PA4207, doi:10.1029/2007PA001564.

Anderson, D. M., and W. L. Prell (1993), A 300 kyr record of upwelling off Oman during the late Quaternary: evidence of the Asian southwest monsoon, *Paleoceanography, 8,* 193–208.

Barker, S., M. Greaves, and H. Elderfield (2003), A study of cleaning procedures used for foraminiferal Mg/Ca paleothermometry, *Geochem. Geophys. Geosyst., 4 (9),* 8407, doi: 10.1029/2003GC000559.

Banakar, V. K., T. Oba, A. R. Chodankar, T. Kuramoto, M. Yamamoto, and M. Minagawa (2005), Monsoon related changes in sea surface productivity and water column denitrification in the Eastern Arabian Sea during the last glacial cycle, *Marine Geology*, *219*, 99-108.

Bemis, B., H. Spero, J. Bijima, and D. W. Lea (1998), Reevaluation of the oxygen isotopic composition of planktonic foraminifera: Experimental results and revised paleotemperature equations, *Paleoceanography*, *13*, 150-160, doi:10.1029/98PA00070.

Cadet, D., and G. Reverdin (1981), Water vapor transport over the Indian Ocean during summer 1975, Tellus, 33, 476-487.

Chodankar, A. R., V. K. Banakar, and T. Oba (2005), Past 100 kyr surface salinity-gradient response in the Eastern Arabian Sea to the summer monsoon variation recorded by $\delta^{18}O$ of *G. sacculifer*, *Global and Planetory Change*, *47,* 135-142.

CLIMAP Project Members (1981), seasonal reconstruction of the Earth's surface at the last glacial maximum, Map Chart ser. MC-36, *Geol. Soc. Am*., Boulder, Colo.

Dahl, A. K., and D. W. Oppo (2006), Sea surface temperature pattern reconstructions in the Arabian Sea, *Paleoceanograpy, 21,* PA1014, doi: 10.1029/2005PA001162.

Delaygue, G., E. Bard, C. Rollion, J. Jouzel, M. Stievenard, J-C. Duplessy, and G. Ganssen (2001) Oxygen isotope/salinity relationship in the northern Indian Ocean, *J. Geophys. Res*., *106*, 4565-4574.

Dekens, P. S., D. W. Lea, D. K. Pak, and H. J. Spero (2002), Core top calibration of Mg/Ca in tropical foraminifera: refining paleo-temperature estimation, *Geochem. Geophys. Geosys. 3,* 1022, 10.1029/2001GC000200.

Duplessy, J. C. (1982), Glacial to interglacial contrast in the northern Indian Ocean, *Nature*, *295,* 464-498.

Emeis, K-C., D. M. Anderson, D. Kroon, and D. Schulz-Bull (1995), Sea-surface temperatures and history of monsoon upwelling in the northwestern Arabian Sea during the last 500,000 years, *Quart. Res.,* 43, 355-361.

Fontugne, M. R., and J. C. Duplessy (1986), Variations of the monsoon regime during the upper Quaternary: Evidence from carbon isotopic record of organic matter in north Indian Ocean sediment cores, *Palaeogeogr. Palaeoclimatol. Palaeoecol., 56,* 69-88.

Gupta, A. K., D. M. Anderson, and J. T. Overpeck (2003), Abrupt changes in the Asian southwest monsoon during the Holocene and their links to the North Atlantic Ocean, *Nature*, *421,* 354-356.

Hastenrath, S., and P. J. Lamb (1979), Climatic Atlas of the Indian Ocean Part I, Surface circulation and climate, University of Wisconsin Press, Madison, pp. 97.

Levitus, S., and T. P. Boyer (1994), World Ocean Atlas 1994. Temperature, vol. 4. NOAA Atlas NESDIS, 4. US Department of Commerce, Washington, DC, pp. 99.

Martinson, D. G., N. G. Pisias, J. D. Hays, J. Imbrie, T. C. Moore, and N. J. Shackleton (1987), Age dating and the orbital theory of the ice ages: development of a high resolution 0 to 300,000-year chronostratigraphy, *Quaternary Research*, *27,* 1-29.

Montegut, C.D., J. Vialard, S.S.C. Shenoi., D. Shankar, F. Durand, C. Ethe, G. Madec (2007), Simulated seasonal and interannual variability of mixed layer heat budget in the northern Indian Ocean. *Journal of Climate,*20, 3249-3268.

Neff, U., S. J. Burns, A. Mangini, M. Mudelsec, D. Fleitmann, and A. Matter (2001), Strong coherence between solar variability and the monsoon in Oman between 9 and 6 kyr ago, *Nature* 411, 290-293.

Naidu, P. D. (1998), Driving forces of Indian summer monsoon on Milankovitch and sub-Milankovitch time scales: A review, *J. Geol. Soc. India*, *52,* 257–272.

Naidu, P. D. (2004), Isotopic evidences of past upwelling intensity in the Arabian Sea, *Global Planet. Change, 40,* 285-293.

Naidu, P. D, and B. A. Malmgren (1995), A 2,200 years periodicity in the Asian monsoon system, *Geophys. Res. Lett., 22,* 2361-2364.

Naidu, P. D, and B. A. Malmgren (1996), A high-resolution record of late Quaternary upwelling along the Oman Margin, Arabian Sea based on planktonic foraminifera, *Paleoceanography, 11,* 129–140.

Naidu, P. D, and B. A. Malmgren (2005), Seasonal sea surface temperature contrast between the Holocene and last glacial period in the western Arabian Sea (Ocean Drilling Project Site 723): Modulated by monsoon upwelling, *Paleoceanography*, *20,* doi: 10.1029/2004PA001078.

Overpeck, J. T., D. M. Anderson, S. Trumbore, and W. L. Prell (1996), The southwest Indian monsoon over the last 18,000 years, *Climate Dynamics, 12,* 213–225.

Prell, W. L. (1984), Variation of monsoonal upwelling: a response to changing solar radiation. In: Hansen JE, Takahashi T (eds.). *Climatic Processes and Climate sensitivity, Am. Geophys. Union, Maurice Ewing Ser.*, *5,* 48-57.

Prell, W. L., and E. V. Campo (1986), Coherent response of Arabian Sea upwelling and pollen transport of late Quaternary monsoonal winds, *Nature*, *323,* 526-528.

Ramesh Kumar, M. R, and P. Schlussel (1998), Air-Sea Interaction over the Indian Ocean During the Two Contrasting Monsoon years 1987 and 1988 Studied with Satellite Data. *Theor. Appl. Climatol*, 60, 219-231.

Rao, K. G., and B. N. Goswami (1988), Interannual variation of sea surface temperature over the Arabian Sea and the INdian monsoon: A new perspective. *Mon. Weat. Rev*. 116, 558-568.

Rashid, H., B. P. Flower, R. Z. Poore, and T. M. Quinn (2007), A ~25ka Indian Ocean monsoon variability record from the Andaman Sea, *Quat. Sci. Review*, *26*, 2586-2597.

Reichart, G. J., L. J. Lourens, and W. J. Zachariasse (1998) Temporal variability in the northern Arabian Sea Oxygen Minimum Zone (OMZ) during the last 225,000 years, *Paleoceanography*, *13*, 607-621.

Rostek, F., G. Ruhland, F. C. Bassinot, P. J. Muller, L. D. Labeyrie, Y. Lancelot, and E. Bard (1993), Reconstructing sea surface temperature and salinity using δ18O and alkenone records, *Nature*, *364*, 319-321.

Rostek, F., E. Bard, L. Beaufort, C. Sonzogni, and G. Ganssen (1997), Sea surface temperature and productivity records for the past 240 kyr in the Arabian Sea, *Deep Sea Res., 44,* 1461-1480.

Saher, M. H., S. J. A. Jung, H. Elderfield, M. J. Greaves, and D. Kroon (2007), Sea surface temperatures of the western Arabian Sea during the last deglaciation, *Paleoceanography*, *22,* PA2208, doi: 10.1029/2006PA001292.

Saher, M. H., F. Rostek, S. J. A. Jung, E. Bard, R. R. Schneider, M. Greaves, G. M. Ganssen, H. Elderfield, and D. Kroon (2009), Western Arabian Sea SST during the penultimate interglacial: A comparision of Uk37 and Mg/Ca paleothermometry, Paleogeography, 24, PA2212, doi:10,1029/2007PA001557.

Sarkar, A., R. Ramesh, S. K. Bhattacharya, and G. Rajagopalan (1989), Oxygen isotope evidence for a stronger winter monsoon current during the last glaciations, *Nature*, *343,* 549-551.

Sarkar, A., R. Ramesh, B. L. K. Somayajulu, R. Agnihotri, and A. J. T. Jull (2000), High resolution Holocene monsoon record from the eastern Arabian Sea, *Earth Planet Sci. Lett., 177,* 209-218.

Schulz, H., U. Von Rad, and H. Erlenkeuser (1998), Correlation between Arabian Sea and Greenland climate oscillations of the past 110,000 years, *Nature, 939*, 54-57.

Shackleton, N. J. (2000), A 100,000 year ice-age cycle identified and found to lag temperature, carbon-dioxide, and orbital eccentricity, *Science*, *289*, 1897-1902.

Shankar, D., P. N. Vinaychandran., A. S. Unnikrishnan (2002), The monsoon currents in the north Indian Ocean, *Prog. Oceanogr*. 52, 63-120

Shukla, J., and D. A. Mooley (1987), Empirical prediction of the summer monsoon over India, *Mon. Weath. Rev. 115*, 695-703.

Sirocko, F., M. Sarnthein, H. Erlenkeuser, H. Lange, M. Arnold, and J. C. Duplessy (1993), Century-scale events in monsoonal climate over the past 24, 000 years, *Nature*, *364*, 322-324.

Southon, J., M. Kashgarian, M. Fontugne, B. Metivier, and W. S. Wyss (2002), Marine reservoir corrections for the Indian Ocean and Southeast Asia, *Radiocarbon*, 44, 167-180.

Thamban, M., V. P. Rao, R. R. Schneider, and P. M. Grootes, (2001), Glacial to Holocene fluctuations in hydrography and productivity along the southwestern continental margin of India, *Palaeogeography, Palaeoclimatology, Palaeoecology*, *165*, 113-127.

Tiwari, M., R. Ramesh, B. L. K. Somayajulu, A. J. T. Jull, and G. S. Burr (2005a), Paleomonsoon precipitation deduced from a sediment core from the equatorial Indian Ocean *Geo-Mar. Lett. 26,* 23-30.

Tiwari, M., R. Ramesh, B. L. K. Somayajulu, A. J. T. Jull, and G. S. Burr (2005b), Early deglacial (19-17 ka) strengthening of the northeast monsoon, *Geophys. Res. Lett. 32,* L19712, doi:10.1029/2005GL024070.

Webster, P. J., V. O. Magana, T. N. Palmer, J. Shukla, R. A. Tomas, M. Yanai, and T. Yasunari (1998), Monsoons: Processes, predictability, and the prospects for prediction, *J. Geophys. Res*., 103, 14,451-14,510.

Weninger, B., O. Joris, and U. Danzeglocke (2006), Calpal-Cologne Radiocarbon Calibration and Paleoclimate Research Package, Universitat zu Koln, Institut fur Ur-und Fruhgeschichte Radiocarbon Laboratory.

Wyrtki, W. (1973), Physical Oceanography of the Indian Ocean. In: *The Biology of the Indian Ocean* (B. Zeitschel, and S. A. Gerlach, Eds) pp. 18-36, Springer-Verlag, New York.

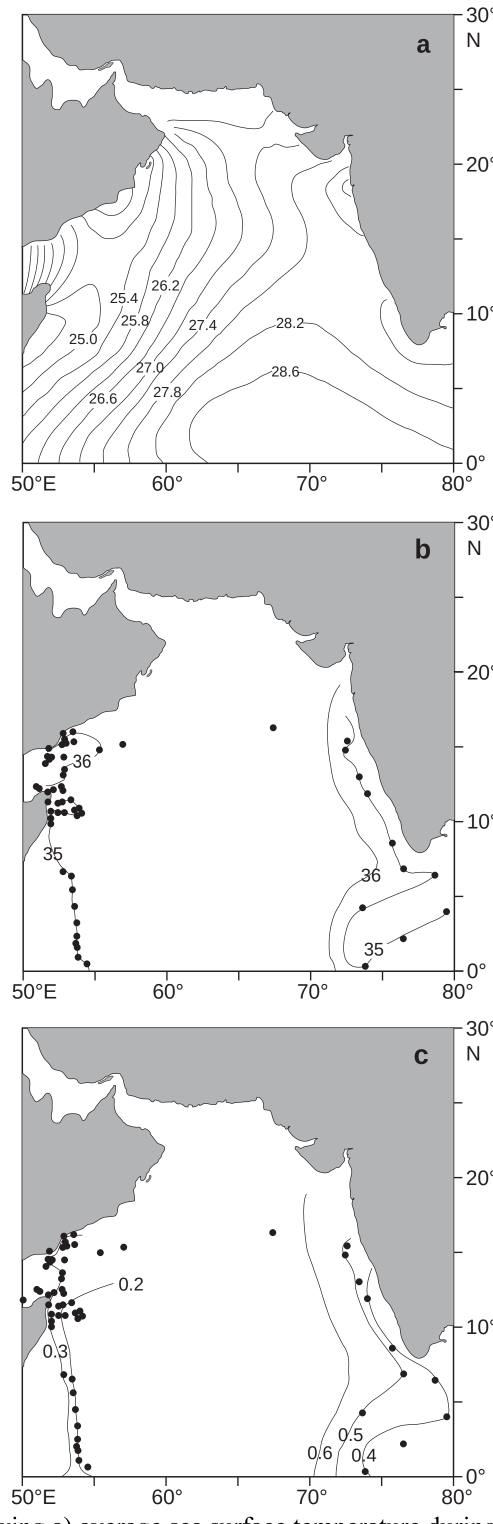

Figure 1. Map of the Arabian Sea showing a) average sea surface temperature during SW monsoon (*Levitus and Boyer*, 1994), b) sea surface salinity during SW monsoon (Joint Global Ocean Flux data, *Dahl and Oppo*, 2006) and c) δ^{18}Ow of sea water during SW monsoon (Joint Global Ocean Flux data, *Dahl and Oppo*, 2006) . Sea surface salinity and δ^{18}Ow show lower values near to the coast as compared to offshore mainly due to SW monsoon rainfall on the Western Ghats drains into the Arabian Sea through numerous rivers and streams resulting salinity gradient from near shore to offshore. Note the dots represent data points based on which contours were drawn.

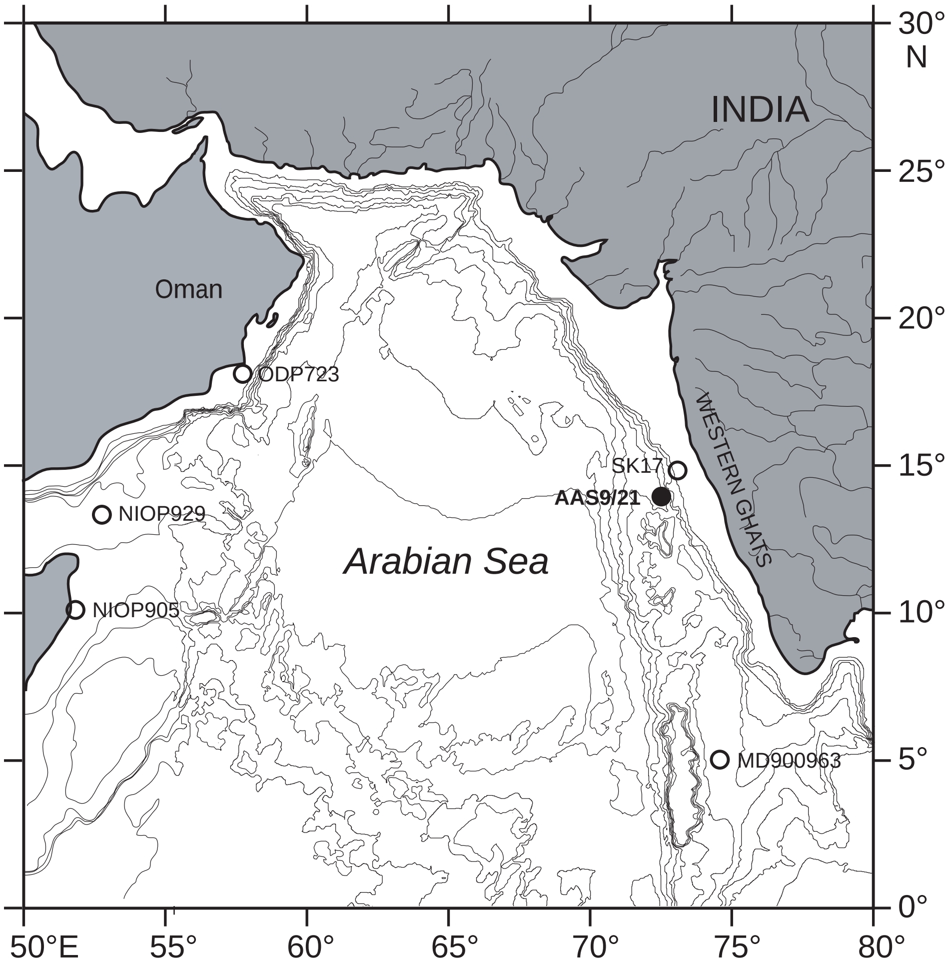

Figure 2. Map showing location of core AAS9/21 and other cores discussed in this paper ODP 723 (*Naidu and Malmgren*, 1995) NIOP 929 (*Saher et al*., 2007) NIOP 905 and SK17 (*Anand et al*., 2008) MD900963 (*Rostek et al*., 1993).

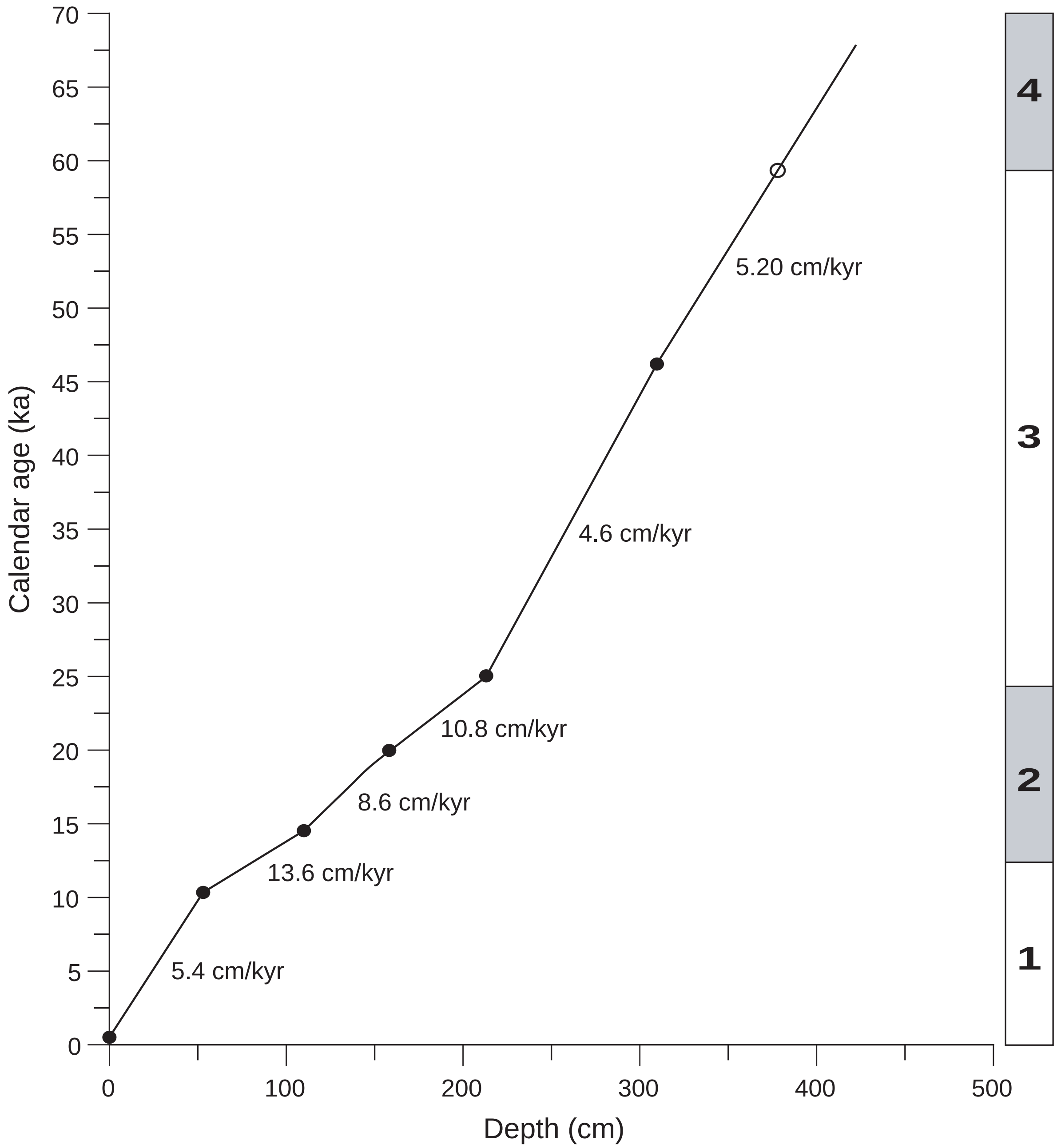

Figure 3. Plot of AMS ^{14}C dates calibrated to calendar age (filled circle) and isotope stage boundary of 3 and 4 (shown with unfilled circle) as a function of depth along with sedimentation rates corresponding between two tie points. Marine Isotope Stages (MIS) are marked on the right panel, glacial stages shows are shaded.

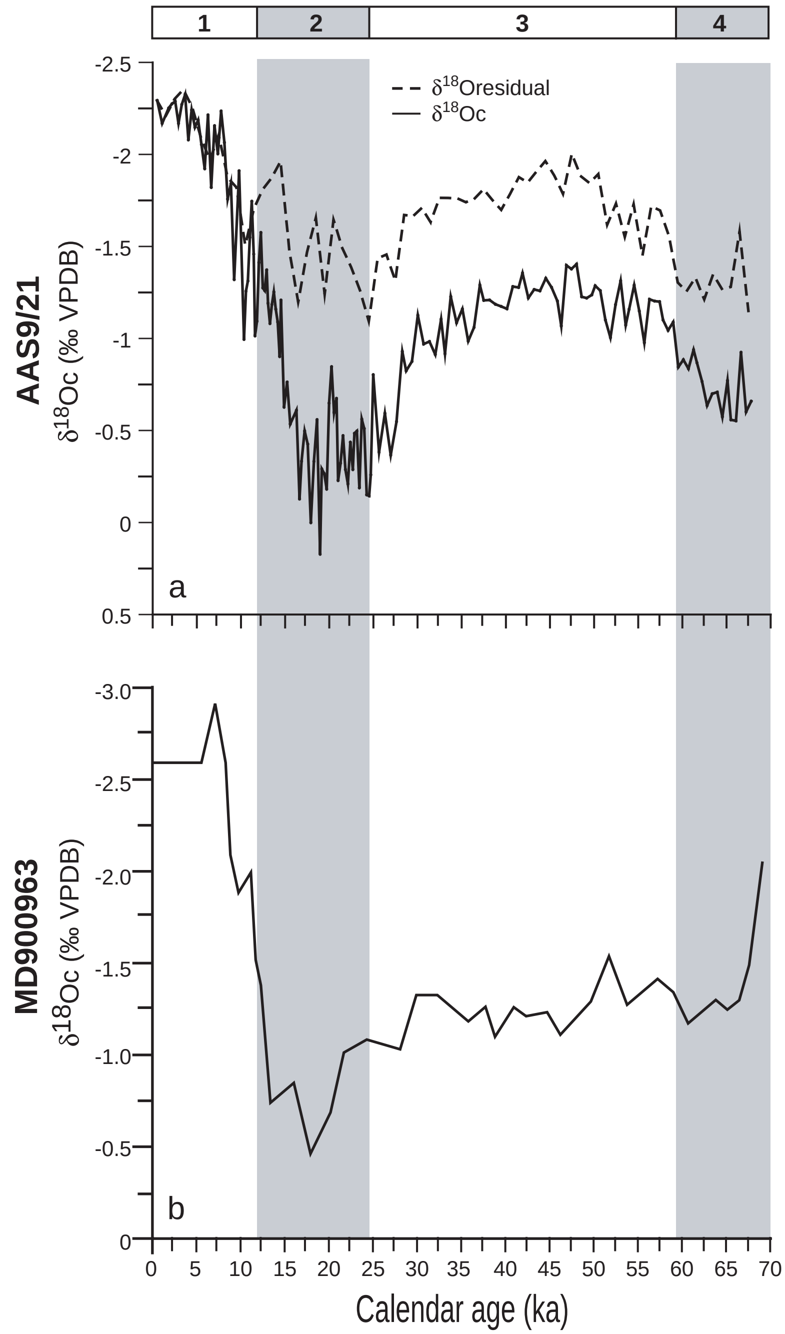

Figure 4. (a)The Oxygen isotope profile of *G. ruber* (δ^{18}Oc) from the core AAS9/21 shown with line and symbol and residual δ^{18}O values are shown with broken line. Residual δ^{18}O values were obtained by subtracting ice volume effect values (*Shackleton*, 2000) from δ^{18}Oc of the AAS9/21core. (b) Oxygen isotope profile of *G. ruber* (δ^{18}Oc) for core MD900963 (*Rostek et al*., 1993). Shaded and un-shaded stages represent glacial and interglacial Marine Isotope Stages (MIS) respectively.

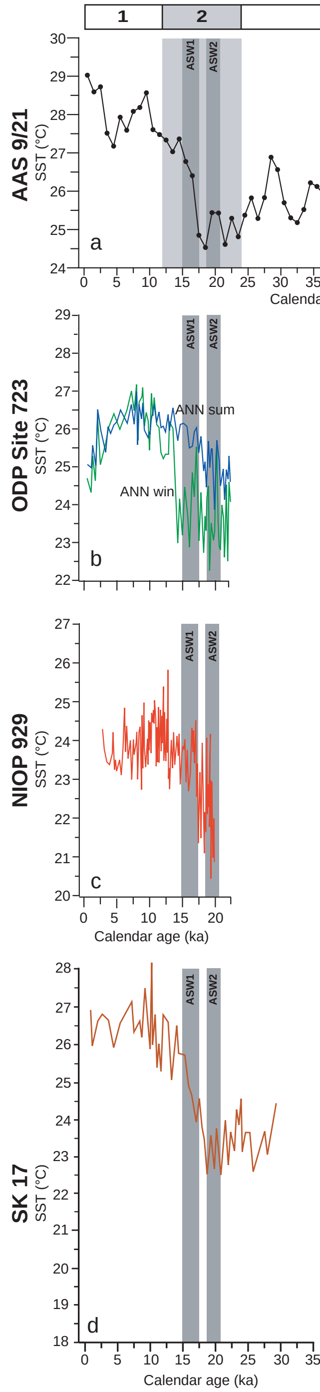

Figure 5. Profiles of sea surface temperature (SST) for core (a) AAS9/21 are compared with SST of (b) ODP 723 (*Naidu and Malmgren*, 2005), (c) NIOP929 (*Saher et al*., 2007), (d) SK17 (*Anand et al*., 2008). Two warm events Arabian Sea Warm Event 1 (ASW1) and Arabian Sea Warm Event 2 (ASW2) were documented during MIS 2. Note ASW 1 event in AAS19/21 and SK17 was a part of deglaciation warming in the EAS. Shaded and un-shaded stages represent glacial and interglacial Marine Isotope Stages (MIS) respectively.

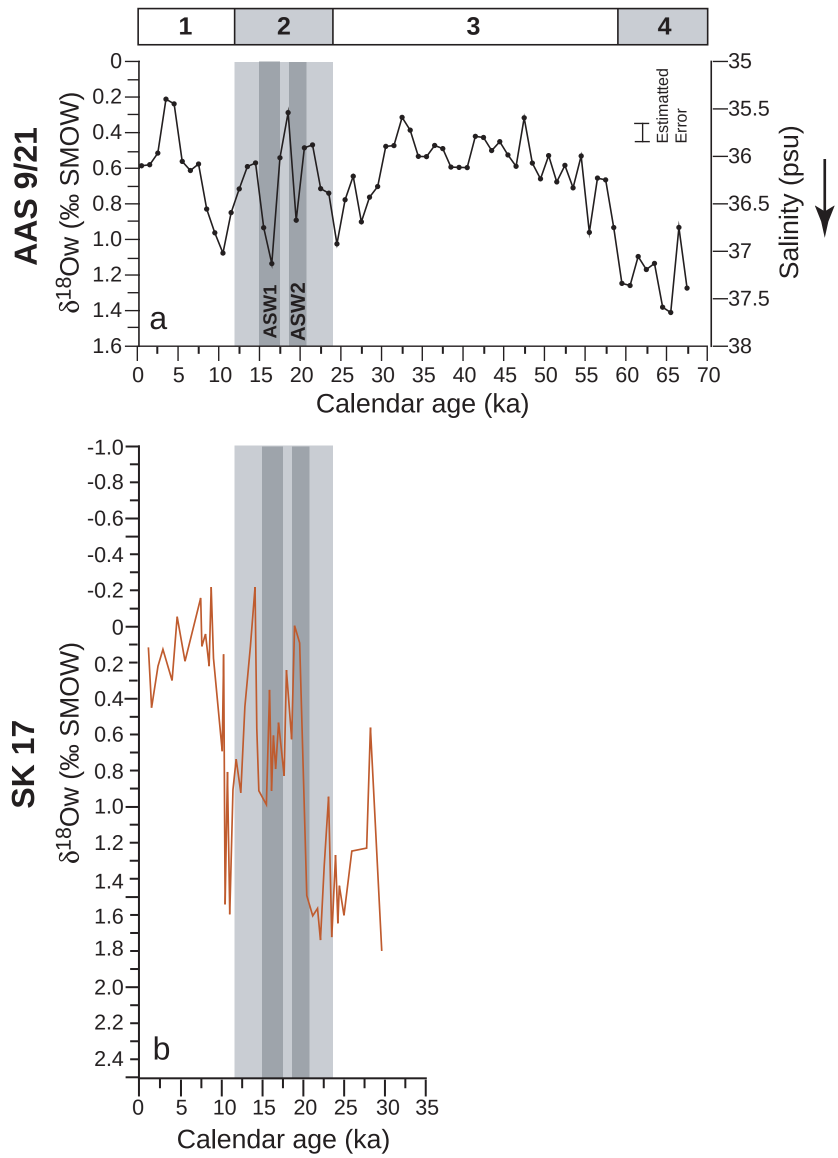

Figure 6. (a) AAS9/21 δ^{18}Ow records are compared with the δ^{18}Ow records of SK17 (b) (*Anand et al*., 2008). Enriched δ^{18}Ow values during ASW1 and ASW2 represent less flow of Bay of Bengal water due to weak NE monsoon strength. Note the exact time of starting and ending of ASW1 and ASW2 in these two cores occurs with $\pm$500 years difference.